Chemical Science

ROYAL SOCIETY OF CHEMISTRY

EDGE ARTICLE

View Article Online
View Journal | View Issue

Cite this: *Chem. Sci.*, 2021, **12**, 2165

All publication charges for this article have been paid for by the Royal Society of Chemistry

Received 2nd November 2020
Accepted 17th December 2020

DOI: 10.1039/d0sc06017h

rsc.li/chemical-science

Supramolecular-induced regiocontrol over the photochemical [4 + 4] cyclodimerization of NHC- or azole-substituted anthracenes†

Sha Bai,‡[a] Li-Li Ma,‡[a] Tao Yang,[c] Fang Wang,[a] Li-Feng Wang,[a] F. Ekkehardt Hahn,[b] Yao-Yu Wang[a] and Ying-Feng Han*[a]

Thanks to the impressive control that microenvironments within enzymes can have over substrates, many biological reactions occur with high regio- and stereoselectivity. However, comparable regio- and stereoselectivity is extremely difficult to achieve for many types of reactions, particularly photochemical cycloaddition reactions in homogeneous solutions. Here, we describe a supramolecular templating strategy that enables photochemical [4 + 4] cycloaddition of 2,6-difunctionalized anthracenes with unique regio- and stereoselectivity and reactivity using a concept known as the supramolecular approach. The reaction of 2,6-azolium substituted anthracenes H_4-L$(PF_6)_2$ (L = **1a–1c**) with Ag_2O yielded complexes *anti*-$[Ag_2L_2](PF_6)_4$ featuring an antiparallel orientation of the anthracene groups. Irradiation of complexes *anti*-$[Ag_2L_2](PF_6)_4$ proceeded under [4 + 4] cycloaddition linking the two anthracene moieties to give cyclodimers *anti*-$[Ag_2(\mathbf{2})](PF_6)_2$. Reaction of 2,6-azole substituted anthracenes with a dinuclear complex [Cl-Au-NHC–NHC-Au-Cl] yields tetranuclear assemblies with the anthracene moieties oriented in *syn*-fashion. Irradiation and demetallation gives a [4 + 4] *syn*-photodimer of two anthracenes. The stereoselectivity of the [4 + 4] cycloaddition between two anthracene moieties is determined by their orientation in the metallosupramolecular assemblies.

Introduction

Supramolecular approaches offer solutions to the problem of preorganization of the orientation and conformation of photoreactive reactants,[1,2] such that efficient photochemical reactions can also be extended to homogeneous systems.[3,4] However, controlling the regio- and stereoselectivity of a photoinduced transformation while maintaining the high reactivity of the photoactive components remains an inherent challenge.[5] For example, in order to improve the selectivity of photochemical [4 + 4] reactions of monosubstituted anthracenes (such as 2-anthracene carboxylic acid), much effort has been directed toward the application of various supramolecular environments.[6–11] Although the photochemical [4 + 4] cycloaddition of anthracene derivatives is one of the well-studied subjects in photochemistry,[12–19] relatively few studies deal with the photodimerization of 2,6-difunctionalized anthracenes.[20] Generally, irradiation of 2,6-difunctionalized anthracene derivatives (**AD**) in solution leads to the formation of two [4 + 4] photodimerization products, the *anti*-**dAD** (mixture of enantiomers) and *syn*-**dAD** (achiral) photodimers (Fig. 1a). To the best of our knowledge, the controlled, selective formation of *anti*-**dAD** or *syn*-**dAD** in solution *via* photochemical [4 + 4] cycloaddition remains relatively unexplored, mainly due to microenvironments for a selective reaction.

Recently, we have demonstrated that NHC-functionalized (NHC = N-heterocyclic carbene) metallacycles are good candidates for efficient supramolecular-controlled photochemical [2 + 2] cycloaddition reactions in solution.[21] We found that the antiparallel arrangement of photoreactive substrates with twisted structures can be formed by using suitable type-I units,[21d] while a parallel arrangement of the reactants can be favored when type-II organometallic clips were employed (Fig. 1b).[21b] In nature, many enzymes accelerate or facilitate reactions with high regio- and stereoselectivity by adjusting their microenvironments in the presence of different substrates. We thus envisaged that the flexibility of supramolecular templates, when appropriately introduced, would facilitate the preorganization of the spatial arrangement of anthracene moieties within their structures. Given the reduced translational, rotational, and conformational freedom of the

[a]*Key Laboratory of Synthetic and Natural Functional Molecule of the Ministry of Education, College of Chemistry and Materials Science, Northwest University, Xi'an 710127, P. R. China. E-mail: yfhan@nwu.edu.cn*

[b]*Institut für Anorganische und Analytische Chemie, Westfälische Wilhelms-Universität Münster, Corrensstraße 30, 48149 Münster, Germany*

[c]*School of Science, MOE Key Laboratory for Non-Equilibrium Synthesis and Modulation of Condensed Matter, Xi'an Jiaotong University, Xi'an 710049, P. R. China*

† Electronic supplementary information (ESI) available. CCDC 1995058, 1995079–1995083 and 2026357. For ESI and crystallographic data in CIF or other electronic format see DOI: 10.1039/d0sc06017h

‡ S. Bai and L.-L. Ma contributed equally to this work.

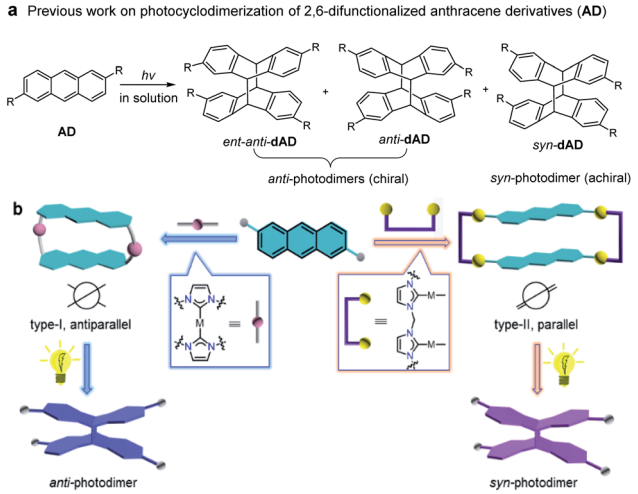

Fig. 1 (a) The mixture of isomeric products obtained by [4 + 4] cycloaddition of 2,6-substituted anthracenes. (b) The supramolecular-template-controlled regioselective [4 + 4] photochemical cycloaddition of 2,6-substituted anthracenes, in which the *anti*-photodimer is an enantiomer.

anthracene moieties and their close proximity within the metallosupramolecular structure, the selective synthesis of *anti*- and *syn*-photodimerization products from assemblies of types-I and -II appears possible. The two different supramolecular architectures should steer the [4 + 4] photochemical reaction of the anthracene groups towards different products with excellent regio- and stereoselectivity.

Herein, we demonstrate that a metallosupramolecular approach depicted in Scheme 1 allows to perform the photochemical [4 + 4] cycloaddition of 2,6-difunctionalized anthracene derivatives in solution with excellent regio- and stereoselectivity. In this supramolecular approach, the reaction outcome is determined by the preorganization of the reacting units rather than by their intrinsic reactivity. Irradiation of the different metallacycles led to the exclusive formation of a specific isomer in each case. The chiral *anti*-photodimers (*anti*-**dAD** and *ent-anti*-**dAD** in 1 : 1 molar ratio) were obtained in high yields after removal of the metal ions from the photoproducts. Notably, *in situ* photolysis of metallarectangles of type-II led to the isolation of the desired achiral *syn*-photodimers (*syn*-**dAD**) without the need for a separate metal-removal step.

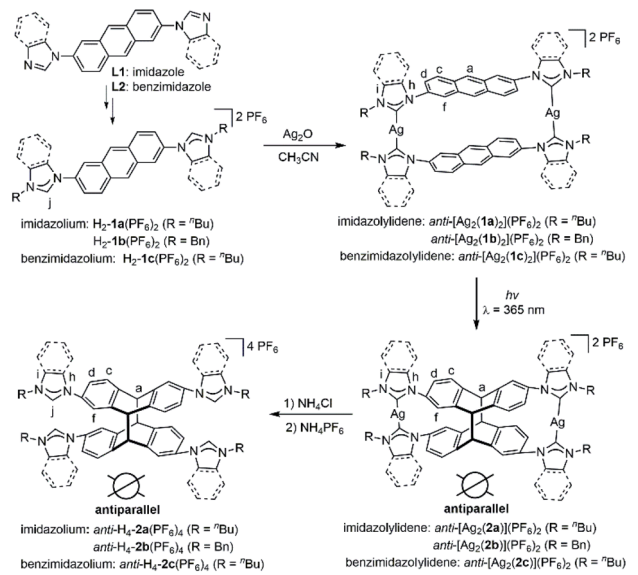

Scheme 1 Metallosupramolecular-controlled synthesis of tetrakisazolium salts *anti*-H_4-**2**$(PF_6)_4$ from complexes *anti*-$[Ag_2(L)_2](PF_6)_2$ by [4 + 4] cycloaddition.

Results and discussion

Synthesis and characterization of *anti*-photodimers from type-I assemblies

The reaction of linear bisimidazolium salts with Ag_2O is known to produce dinuclear tetracarbene complexes $[Ag_2L_2]$.[21] The 2,6-anthracene-bridged bisimidazolium salts H_2-**L**$(PF_6)_2$ (**L** = **1a**,**b**) and bisbenzimidazolium salt H_2-**L**$(PF_6)_2$ (**L** = **1c**) were synthesized from 2,6-di(1*H*-imidazol-1-yl)anthracene (**L1**) and 2,6-bis(1*H*-benzo[*d*]imidazol-1-yl)anthracene (**L2**) by *N*-alkylation and anion exchange (Scheme 1). The bis(benz)imidazole anthracenes **L1** and **L2** were synthesized in good yields from 2,6-dibromoanthracene and imidazole or benzimidazole by an Ullmann coupling reaction. The molecular structures of **L1** and **L2** were determined by X-ray diffraction studies (Fig. S1†). The ligands H_2-**L**$(PF_6)_2$ (**L** = **1a–c**) were characterized by NMR spectroscopy and electrospray ionization mass spectrometry (ESI-MS) (Fig. S11–S19†). Surprisingly, a solution of H_2-**1a**$(PF_6)_2$ was found to be photostable upon exposure to UV light ($\lambda = 365$ nm) for 6 h. The anthracene motifs were found to be photoactive in solution only after metallation of the azolium groups with Ag^I ions in a metallosupramolecular assembly.

The reaction of the 2,6-difunctionalized anthracenes H_2-**L**$(PF_6)_2$ (**L** = **1a–c**) with Ag_2O under exclusion of light in acetonitrile afforded the disilver(I) tetracarbene complexes *anti*-$[Ag_2(\mathbf{L})_2](PF_6)_2$ (**L** = **1a–c**) in good yields (Scheme 1). The ^{1}H NMR spectrum of *anti*-$[Ag_2(\mathbf{1a})_2](PF_6)_2$ showed a single set of signals with upfield shifts observed in the aromatic region relative to salt H_2-**1a**$(PF_6)_2$ (Fig. 2a and b). In addition, the disappearance of the imidazolium C2–H resonance (labeled H_j) was noted in the ^{1}H NMR spectrum upon metallation of H_2-**1a**$(PF_6)_2$ together with the appearance of the typical resonance at $\delta = 178.4$ ppm for the Ag^I-bound carbene carbon atoms in the $^{13}C\{^1H\}$ NMR spectrum (Fig. S21†). Similarly, the formation of carbene complexes *anti*-$[Ag_2(\mathbf{L})_2](PF_6)_2$ (**L** = **1b,c**) were monitored by NMR spectroscopy (Fig. S26–S30† for *anti*-$[Ag_2(\mathbf{1b})_2](PF_6)_2$ and ESI Fig. S32 and S33† for *anti*-$[Ag_2(\mathbf{1c})_2](PF_6)_2$). The formation of *anti*-$[Ag_2(\mathbf{L})_2](PF_6)_2$ (**L** = **1a–c**) was also confirmed by ESI-MS data. The HR-ESI mass spectra (positive ion mode) of the complexes showed the highest intensity peaks at m/z = 530.1664 (calcd for *anti*-$[Ag_2(\mathbf{1a})_2]^{2+}$ 530.1517), at m/z = 598.1185 (calcd for *anti*-$[Ag_2(\mathbf{1b})_2]^{2+}$ 598.1206) and at m/z = 630.1703 (calcd for *anti*-$[Ag_2(\mathbf{1c})_2]^{2+}$ 630.1832) with the correct isotopic patterns.

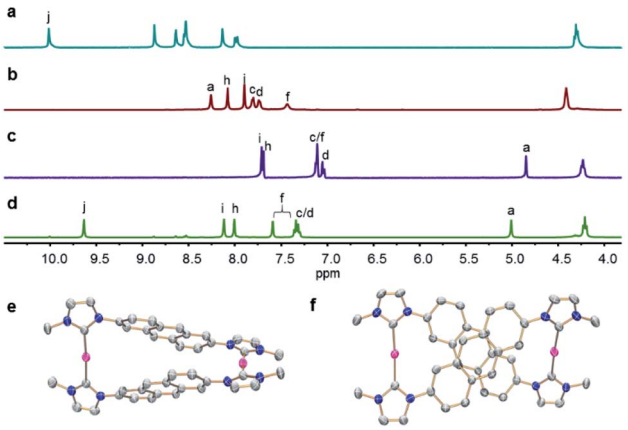

Fig. 2 Sections of the ^{1}H NMR spectra in [D$_6$]DMSO of (a) bisimidazolium salt H$_2$-**1a**(PF$_6$)$_2$; (b) complex *anti*-[Ag$_2$(**1a**)$_2$](PF$_6$)$_2$ before irradiation; (c) complex *anti*-[Ag$_2$(**2a**)](PF$_6$)$_2$ obtained after irradiation; (d) tetrakisimidazolium salt *anti*-H$_4$-**2a**(PF$_6$)$_4$. (e) Side and (f) top views of complex cation *anti*-[Ag$_2$(**1a**)$_2$]$^{2+}$ as determined by X-ray diffraction (N, blue; C, grey; Ag, purple) with hydrogen atoms omitted for clarity and only the first atom of each *N*-substituent is depicted.

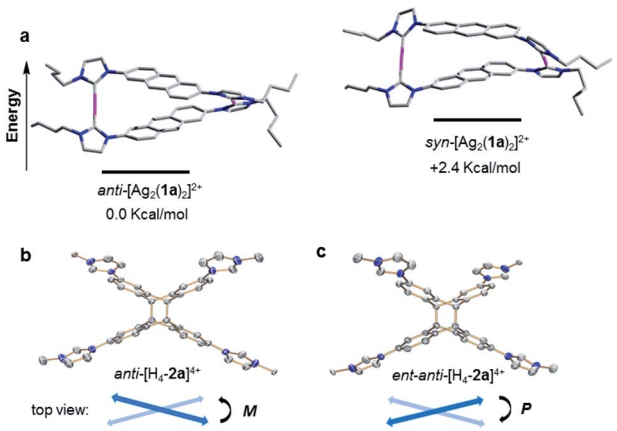

Fig. 3 (a) DFT calculated structures (in CH$_3$CN) and relative energies of *anti*-[Ag$_2$(**1a**)$_2$]$^{2+}$ (left) and *syn*-[Ag$_2$(**1a**)$_2$]$^{2+}$ (right). (b) Side view of the *M*-isomer of enantiomer of *anti*-[H$_4$-**2a**]$^{4+}$ and (c) side view of the *P*-isomer of *ent-anti*-[H$_4$-**2a**]$^{4+}$ as determined by single-crystal X-ray diffraction (N, blue; C, grey; Ag, purple). Hydrogen atoms have been omitted for clarity, and only the first atom of each *N*-substituent is depicted.

Single crystals of *anti*-[Ag$_2$(**1a**)$_2$](BPh$_4$)$_2$ were obtained by adding of an excess of NaBPh$_4$ to a CH$_3$CN solution of *anti*-[Ag$_2$(**1a**)$_2$](PF$_6$)$_2$ and allowing the solution to stand at ambient temperature for several days. The X-ray diffraction analysis confirmed the formation of the disilver metallacycle (Fig. 2e and f). The coordination geometry around the silver(I) atoms is almost linear and the Ag–C$_{NHC}$ distances (2.075(2)–2.079(2) Å) fall in the range previously reported for related silver polycarbene assemblies.[21] The nonbonding Ag···Ag distance measures 10.925(3) Å.

As shown in Fig. 2f, the two anthracene skeletons are arranged in the expected antiparallel conformation, forming an X-shaped arrangement as seen from the top view. The distance between two central aromatic rings measures about 3.57 Å, which is within Schmidt's range proposed for a photoinduced cycloaddition reaction.[22] It is worth mentioning that the intermolecular interactions of adjacent *anti*-[Ag$_2$(**1a**)$_2$](PF$_6$)$_2$ assemblies were not observed in the unit cell, thus preventing intermolecular [4 + 4] photochemical reactions.

A computational study was performed to gain insight into the preferred formation of complex *anti*-[Ag$_2$(**1a**)$_2$]$^{2+}$ with the antiparallel orientation of the anthracene groups in solution. Density-functional theory (DFT) calculations at the BP86-D3(BJ)/def2-TZVPP level (see ESI† for details) revealed that the *anti*-[Ag$_2$(**1a**)$_2$]$^{2+}$ species is thermodynamically more stable in CH$_3$CN solution than the *syn*-isomer (+2.4 kcal mol^{-1}, Fig. 3a). The calculated geometry of the *anti*-isomer matches the geometry of cation *anti*-[Ag$_2$(**1a**)$_2$]$^{2+}$ determined by X-ray diffraction. Further calculations indicated that the rotation of the anthracene unit in *anti*-[Ag$_2$(**1a**)$_2$]$^{2+}$ to give *syn*-[Ag$_2$(**1a**)$_2$]$^{2+}$ features a high energy barrier, suggesting that this isomerization is not feasible.

Next, the photochemical [4 + 4] cycloaddition of the anthracene units within metallacycles *anti*-[Ag$_2$(**L**)$_2$](PF$_6$)$_2$ (**L** = **1a–c**) was investigated. A [D$_6$]DMSO solution of metallacycle *anti*-[Ag$_2$(**1a**)$_2$](PF$_6$)$_2$ (c = 0.04 M) was irradiated with UV light (λ = 365 nm) at ambient temperature. ^{1}H NMR monitoring showed the quantitative conversion of *anti*-[Ag$_2$(**1a**)$_2$](PF$_6$)$_2$ into a new single product after 30 min. Upon irradiation, the singlet resonance assigned to the H$_a$ protons of *anti*-[Ag$_2$(**1a**)$_2$](PF$_6$)$_2$ at δ = 8.26 ppm disappeared (Fig. 2b) and a new singlet appeared at δ = 4.86 ppm, which can be assigned to H$_a$ of the newly formed photodimer (Fig. 2c). No mass change was observed upon irradiation by mass spectrometry, confirming the intramolecular [4 + 4] photodimerization within the assembly as the proceeding reaction (Fig. S25 and S43†). It should be noted that the photodimerization proceeded under mild conditions without exclusion of oxygen. The photochemical transformation can also be monitored by UV/Vis and fluorescence spectroscopy. The UV/Vis spectrum of *anti*-[Ag$_2$(**1a**)$_2$](PF$_6$)$_2$ was measured in acetonitrile solution and exhibited a series of vibrationally spaced bands at wavelengths of λ = 350–410 nm, which are assigned to the characteristic π–π* absorption of anthracene systems (Fig. S81†). Irradiation into these bands would lead to the [4 + 4] photodimerization of the anthracene units, accompanied by the disappearance of these characteristic bands. Comparison of the fluorescence spectra of *anti*-[Ag$_2$(**1a**)$_2$](PF$_6$)$_2$ before and after photodimerization exhibited a significantly decrease in the intensity for the photodimer *anti*-[Ag$_2$(**2a**)](PF$_6$)$_2$, attributed to the reduction of π–π stacking interactions of adjacent anthracene units (Fig. S82†).

Under the conditions described above, complex *anti*-[Ag$_2$(**1b**)$_2$](PF$_6$)$_2$ featuring *N*-benzyl groups at the NHC pendants reacted upon irradiation over 25 min to give the quantitatively the photodimer *anti*-[Ag$_2$(**2b**)](PF$_6$)$_2$ (Fig. S2†). The benzimidazolin-2-ylidene disilver complex *anti*-[Ag$_2$(**1c**)$_2$](PF$_6$)$_2$ also yielded photodimer *anti*-[Ag$_2$(**2c**)](PF$_6$)$_2$ after irradiation for 45 min (Fig. S3†). Combined multinuclear and two-dimensional NMR and ESI-MS experiments confirmed the formation of the dinuclear photoproducts *anti*-[Ag$_2$(**L**)](PF$_6$)$_2$ (**L** = **2a–c**).

Finally, the free tetrakisimidazolium salt *anti*-H_4-**2a**$(PF_6)_4$ has been readily obtained through demetallation and anion exchange by treating *anti*-[Ag_2(**2a**)]$(PF_6)_2$ with NH_4Cl and NH_4PF_6 in methanol. The metal-free tetrakisimidazolium salt *anti*-H_4-**2a**$(PF_6)_4$ was isolated as colorless crystals in 84% yield by slow diffusion of ethyl ether into a solution of *anti*-H_4-**2a**$(PF_6)_4$ in methanol/acetonitrile at ambient temperature. The ^{1}H NMR spectrum suggested the presence of a single highly symmetrical species (Fig. 2d). The molecular structure of *anti*-H_4-**2a**$(PF_6)_4$ was unambiguously determined by X-ray crystallography (Fig. 3b and c). As expected, the *anti*-photodimer was obtained as a pair of *P* and *M* enantiomers (the "*P*/*M*" chirality is defined as the right- or left-handed screw arrangement of the longer axes of the anthracenes). Due to the generated 1,4-cyclohexadiene rings, both anthracene planes are slightly bent and the newly formed σ-bonds are rather long (up to 1.612(5) Å), which is consistent with previously reported similar compounds.[23]

Synthesis and characterization of *syn*-photodimers from type-II assemblies

Encouraged by the previously described results, the photochemical conversion of the type-II assemblies (Fig. 1) was studied next. The combination of two organometallic digold clips **3** and two linear 2,6-imidazole-substituted anthracenes **L1** in the presence of AgOTf resulted in the formation of the tetranuclear metallacycle *syn*-[**4a**](OTf)$_4$ in good yield (Scheme 2). NMR spectroscopy revealed downfield shifts of the imidazole proton resonances upon formation of metallacycle *syn*-[**4a**](OTf)$_4$ caused by the loss of electron density upon the coordination of the imidazole nitrogen atoms to the Au^I centers (Fig. 4a and b). The ESI-MS spectrum (positive ion mode) provided further support for the formation of *syn*-[**4a**](OTf)$_4$ by showing high-intensity peaks at $m/z = 1113.1998$ (calcd for [*syn*-[**4a**](OTf)$_2$]$^{2+}$ 1113.2065), 692.4965 (calcd for [*syn*-[**4a**](OTf)]$^{3+}$ 692.4868) and 482.1455 (calcd for [*syn*-[**4a**]]$^{4+}$ 482.1270). The peaks were isotopically resolved and the results are in perfect agreement with the theoretical distribution (Fig. S40†). Since attempts to obtain X-ray quality crystals of the complex *syn*-[**4a**](OTf)$_4$ failed, DFT calculations were performed in order to determine the relative energies of *syn*-[**4a**]$^{4+}$ and *anti*-[**4a**]$^{4+}$ regioisomers. These calculations suggested that the *syn*-[**4a**]$^{4+}$ rectangle is the thermodynamically favored species by -1.6 kcal/mol^{-1} (Fig. 4f). A rotation of the anthracenes and thus the isomerization *syn*-[**4a**]$^{4+}$ to *anti*-[**4a**]$^{4+}$ is energetically unfavorable.

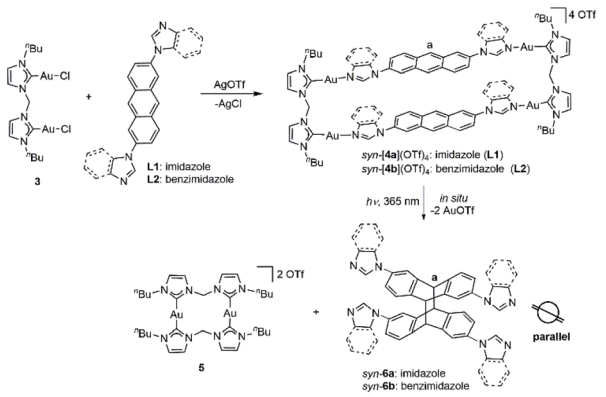

Scheme 2 Synthesis of metallarectangles *syn*-[**4a**](OTf)$_4$ and *syn*-[**4b**](OTf)$_4$ and their [4 + 4] photocycloaddition to afford photodimers *syn*-**6a** and *syn*-**6b**.

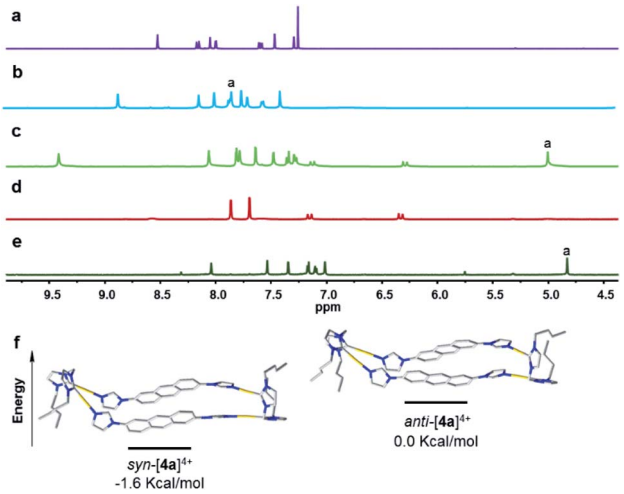

Fig. 4 Sections of the ^{1}H NMR spectra of (a) **L1** in $CDCl_3$; (b and c) complex *syn*-[**4a**](OTf)$_4$ before and after irradiation in [D_6]DMSO; (d) complex **5** in [D_6]DMSO; (e) photodimer *syn*-**6a** in [D_6]DMSO. (f) Energy diagram with DFT calculated structures of *syn*-[**4a**]$^{4+}$ (left), *anti*-[**4a**]$^{4+}$ (right). The energies of the respective metallarectangles were calculated according to equations described in the ESI† (N, blue; C, grey; Au, yellow).

Next metallarectangle *syn*-[**4a**](OTf)$_4$ dissolved in [D_6]DMSO ($c = 5.6 \times 10^{-3}$ M) and irradiated ($\lambda = 365$ nm) in order to investigate the [4 + 4] cycloaddition of this derivative. Monitoring by ^{1}H NMR spectroscopy revealed the complete disappearance of the signal assigned to proton H_a of *syn*-[**4a**](OTf)$_4$ at $\delta = 7.81$ ppm (Fig. 4b) after 3 hours of irradiation. Over this period a new singlet signal at $\delta = 5.01$ ppm appeared, which can be assigned to the H_a resonance of the newly formed photodimer product *syn*-**6a** (Fig. 4c). In line with our previously reported results,[21b] the purely organic compound *syn*-**6a** was formed under extrusion of the known dinuclear gold(I) species **5** (Fig. 4d and e). The organic photodimer *syn*-**6a** was identified by NMR spectroscopy and ESI-MS analysis (Fig. S61 and S62†).

Single crystals of *syn*-**6a** were obtained by slow diffusion of ethyl ether into a solution of the compound in a solvent mixture of dichloromethane and methanol at ambient temperature in 85% yield. The molecular structure and the *syn*-conformation of the photodimer was unambiguously determined by X-ray crystallography (Fig. 5a and b). Importantly, the conformation of *syn*-**6a** is consistent with the conformation that was calculated to be the thermodynamically favored tetranuclear complex cation *syn*-[**4a**]$^{4+}$ (Fig. 4f). In addition, a tetranuclear metallarectangle was constructed from 2 equiv. each of **L2** and **3** (Scheme 2). This self-assembly yielded complex *syn*-[**4b**](OTf)$_4$ which upon irradiation gave the photodimer *syn*-**6b** (Fig. 5c and d).

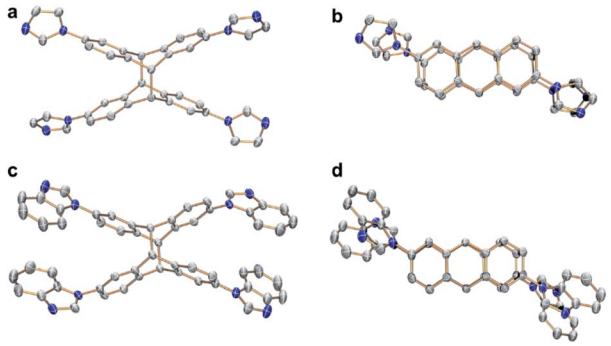

Fig. 5 (a) Side and (b) top views of *syn*-**6a** as determined by single-crystal X-ray diffraction. (c) Side and (d) top views of *syn*-**6b** (N, blue; C, grey). Hydrogen atoms have been omitted for clarity.

The tetrakisimidazole compounds *syn*-**6a** and *syn*-**6b** can be further functionalized at the imidazole moiety. Tetrakis-*N*-alkylation, for example, would lead to new tetrakisimidazolium salts which could be used for the preparation of unprecedented tetra-NHC complexes. We therefore investigated the preparation of a disilver tetracarbene complex from *syn*-**6a**, a complex which would be attainable only with immense difficulties by organic chemistry procedures.

Tetrakis-*N*-alkylation of the metal-free compound *syn*-**6a** readily afforded the tetrakisimidazolium NHC-precursor *syn*-H_4-**7a**$(PF_6)_4$ with retention of the *syn*-conformation as confirmed by X-ray diffraction (Fig. 6a) and ^{1}H NMR spectroscopy (Fig. 6c). The photodimer *syn*-**6a** exhibited high thermal stability during the *N*-alkylation which proceeded at 110 °C for 36 h. The subsequent reaction of *syn*-H_4-**7a**$(PF_6)_4$ with Ag_2O led straightforward to the formation of the dinuclear tetracarbene silver complex *syn*-[Ag_2(**7a**)]$(PF_6)_2$ in high yield. This complex was fully characterized by ^{1}H NMR spectroscopy showing the disappearance of the resonance for the imidazolium C2–H protons (Fig. 6e) and by ^{13}C and ESI-MS analysis (Fig. S75–S80†).

In addition, Fig. 6b depicts the ^{1}H NMR spectra of tetrakisimidazolium salts *anti*-H_4-**2a**$(PF_6)_4$ which was obtained by demetallation of complex *anti*-[Ag_2(**2a**)]$(PF_6)_2$ (Fig. 6d) both featuring the *anti*-arrangement of the anthracene groups. Comparison of the ^{1}H NMR spectra of the *syn*-derivatives *syn*-H_4-**7a**$(PF_6)_4$ and *syn*-[Ag_2(**7a**)]$(PF_6)_2$ to those of the *anti*-derivatives *anti*-H_4-**2a**$(PF_6)_4$ and *anti*-[Ag_2(**2a**)]$(PF_6)_2$ reveals significant differences both for the tetrakisimidazolium salts as well as for the dinuclear silver complexes. These differences between the *syn*- and *anti*-photodimers may constitute a useful feature for the identification of stereoisomers in photochemical [4 + 4] dimerization of anthracene derivatives.

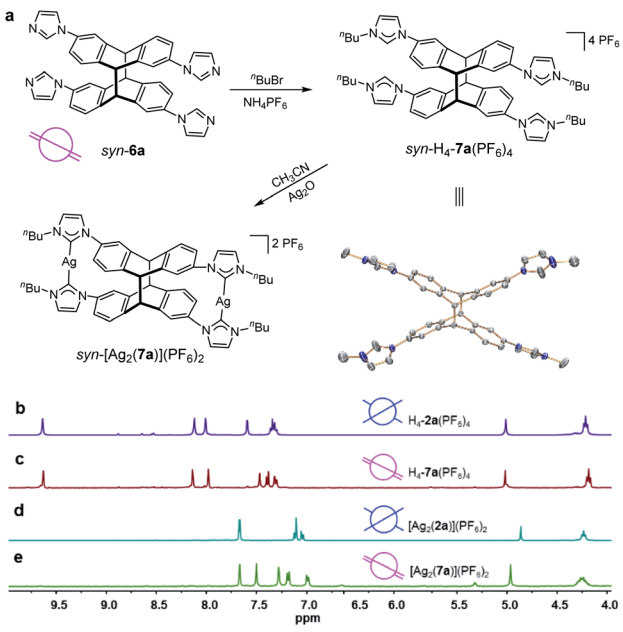

Fig. 6 (a) Synthesis of *syn*-H_4-**7a**$(PF_6)_4$ and of tetra-NHC complex *syn*-[Ag_2(**7a**)]$(PF_6)_2$ and molecular structure of the tetracation *syn*-[H_4-**7a**]$^{4+}$ (N, blue; C, grey). Hydrogen atoms have been omitted for clarity and only the first atom of each *N*-substituent is depicted. Sections of the ^{1}H NMR spectra of (b) tetrakisimidazolium salt *anti*-H_4-**2a**$(PF_6)_4$; (c) tetrakisimidazolium salt *syn*-H_4-**7a**$(PF_6)_4$; (d) complex *anti*-[Ag_2(**2a**)]$(PF_6)_2$; (e) complex *syn*-[Ag_2(**7a**)]$(PF_6)_2$ (all spectra were recorded in [D_6]DMSO).

Conclusions

In summary, we have developed a supramolecular approach that enables the photochemical [4 + 4] cycloaddition of 2,6-difunctionalized anthracene derivatives with excellent regio- and stereoselectivity based on the preorganization of the reactants in metallosupramolecular assemblies. By using different metal templates for the construction of the assemblies, the spatial arrangement and orientation of anthracene units (anti-parallel or parallel) can be controlled, allowing subsequently the exclusive generation of either the *anti*- or *syn*-photodimer isomers. In addition, DFT calculations indicated that the geometric constraints imposed by the metal template and ligand components act synergistically to afford the specific isomer. Thus, our results provide promising approaches for accessing functional organic molecules with interesting and useful characteristics through the modification of supramolecular assemblies. Given the simplicity and high efficiency of the described strategy, we envisage this paradigm system could be considered as a key feature for new photo-induced material designs with different applications.

Conflicts of interest

There are no conflicts to declare.

Acknowledgements

The authors gratefully acknowledge financial support from the NSFC (grant no. 22025107, 21722105, 21771146), the National Youth Top-notch Talent Support Program of China, the Key Science and Technology Innovation Team of Shaanxi Province (2019TD-007, 2019JLZ-02), and the FM & EM International Joint Laboratory of Northwest University.

Notes and references

1 (*a*) L. R. MacGillivray, G. S. Papaefstathiou, T. Friščić, T. D. Hamilton, D.-K. Bučar, Q. Chu, D. B. Varshney and I. G. Georgiev, *Acc. Chem. Res.*, 2008, **41**, 280–291; (*b*) G. K. Kole and J. J. Vittal, *Chem. Soc. Rev.*, 2013, **42**, 1755–1775; (*c*) K. Biradha and R. Santra, *Chem. Soc. Rev.*, 2013, **42**, 950–967; (*d*) Y. Sonoda, *Molecules*, 2011, **16**, 119–148.

2 (*a*) M.-F. Wang, Y. Mi, F.-L. Hu, Z. Niu, X.-H. Yin, Q. Huang, H.-F. Wang and J.-P. Lang, *J. Am. Chem. Soc.*, 2020, **142**, 700–704; (*b*) Z. Liu, C. Zhou, T. Lei, X.-L. Nan, B. Chen, C.-H. Tung and L.-Z. Wu, *CCS Chem.*, 2019, **1**, 582–588; (*c*) M. Tu, H. Reinsch, S. Rodríguez-Hermida, R. Verbeke, T. Stassin, W. Egger, M. Dickmann, B. Dieu, J. Hofkens, I. F. J. Vankelecom, N. Stock and R. Ameloot, *Angew. Chem., Int. Ed.*, 2019, **58**, 2423–2427; (*d*) S. Kusaka, A. Kiyose, H. Sato, Y. Hijikata, A. Hori, Y. Ma and R. Matsuda, *J. Am. Chem. Soc.*, 2019, **141**, 15742–15746; (*e*) F.-L. Hu, Y. Mi, C. Zhu, B. F. Abrahams, P. Braunstein and J.-P. Lang, *Angew. Chem., Int. Ed.*, 2018, **57**, 12696–12701; (*f*) M. A. Sinnwell and L. R. MacGillivray, *Angew. Chem., Int. Ed.*, 2016, **55**, 3477–3480; (*g*) S. Das, N. Okamura, S. Yagi and A. Ajayaghosh, *J. Am. Chem. Soc.*, 2019, **141**, 5635–5639.

3 (*a*) C.-H. Tung, L.-Z. Wu, L.-P. Zhang and B. Chen, *Acc. Chem. Res.*, 2003, **36**, 39–47; (*b*) J. Svoboda and B. König, *Chem. Rev.*, 2006, **106**, 5413–5430; (*c*) B. Bibal, C. Mongin and D. M. Bassani, *Chem. Soc. Rev.*, 2014, **43**, 4179–4198; (*d*) V. Ramamurthy and S. Gupta, *Chem. Soc. Rev.*, 2015, **44**, 119–135; (*e*) V. Ramamurthy and J. Sivaguru, *Chem. Rev.*, 2016, **116**, 9914–9993.

4 (*a*) Y. Zhou, H.-Y. Zhang, Z.-Y. Zhang and Y. Liu, *J. Am. Chem. Soc.*, 2017, **139**, 7168–7171; (*b*) I. Šalitroš, O. Fuhr, M. Gál, M. Valášek and M. Ruben, *Chem.–Eur. J.*, 2017, **23**, 10100–10109; (*c*) G. Fukuhara, K. Iida, Y. Kawanami, H. Tanaka, T. Mori and Y. Inoue, *J. Am. Chem. Soc.*, 2015, **137**, 15007–15014; (*d*) C. P. Carvalho, Z. Domínguez, J. P. D. Silvab and U. Pischel, *Chem. Commun.*, 2015, **51**, 2698–2701; (*e*) C.-K. Liang, J.-P. Desvergne and D. M. Bassani, *Photochem. Photobiol. Sci.*, 2014, **13**, 316–323; (*f*) S. Bringmann, R. Brodbeck, R. Hartmann, C. Schäfer and J. Mattay, *Org. Biomol. Chem.*, 2011, **9**, 7491–7499.

5 (*a*) Y. V. Pol, R. Suau, E. Perez-Inestrosa and D. M. Bassani, *Chem. Commun.*, 2004, 1270–1271; (*b*) J. Paradies, I. Greger, G. Kehr, G. Erker, K. Bergander and R. Fröhlich, *Angew. Chem., Int. Ed.*, 2006, **45**, 7630–7633; (*c*) R. Brimioulle and T. Bach, *Science*, 2013, **342**, 840–843; (*d*) J.-J. Liu, G.-C. Zhang, S. Kwak, E. J. Oh, E. J. Yun, K. Chomvong, J. H. D. Cate and Y.-S. Jin, *Nat. Commun.*, 2019, **10**, 1356–1363; (*e*) T. Dünnebacke, K. K. Kartha, J. M. Wiest, R. Q. Albuquerque and G. Fernández, *Chem. Sci.*, 2020, **11**, 10405–10413.

6 F. Biedermann, I. Ross and O. A. Scherman, *Polym. Chem.*, 2014, **5**, 5375–5382.

7 (*a*) C. Yang, T. Mori, Y. Origane, Y. H. Ko, N. Selvapalam, K. Kim and Y. Inoue, *J. Am. Chem. Soc.*, 2008, **130**, 8574–8575; (*b*) J. Ji, W. Wu, W. Liang, G. Cheng, R. Matsushita, Z. Yan, X. Wei, M. Rao, D.-Q. Yuan, G. Fukuhara, T. Mori, Y. Inoue and C. Yang, *J. Am. Chem. Soc.*, 2019, **141**, 9225–9238; (*c*) X. Wei, A. M. Raj, J. Ji, W. Wu, G. B. Veerakanellore, C. Yang and V. Ramamurthy, *Org. Lett.*, 2019, **21**, 7868–7872.

8 L. S. Kaanumalle, C. L. D. Gibb, B. C. Gibb and V. Ramamurthy, *J. Am. Chem. Soc.*, 2005, **127**, 3674–3675.

9 A. Dawn, N. Fujita, S. Haraguchi, K. Sada and S. Shinkai, *Chem. Commun.*, 2009, 2100–2102.

10 X. Q. Wei, J. J. Liu, G.-J. Xia, J. H. Deng, P. Sun, J. J. Chruma, W. H. Wu, C. Yang, Y.-G. Wang and Z. F. Huang, *Nat. Chem.*, 2020, **12**, 551–559.

11 (*a*) M. Nishijima, T. Wada, T. Mori, T. C. S. Pace, C. Bohne and Y. Inoue, *J. Am. Chem. Soc.*, 2007, **129**, 3478–3479; (*b*) K. Bando, T. Zako, M. Sakono, M. Maeda, T. Wada, M. Nishijima, G. Fukuhara, C. Yang, T. Mori, T. C. S. Pace, C. Bohne and Y. Inoue, *Photochem. Photobiol. Sci.*, 2010, **9**, 655–660.

12 T. Zdobinsky, P. S. Maiti and R. Klajn, *J. Am. Chem. Soc.*, 2014, **136**, 2711–2714.

13 J. Manchester, D. M. Bassani, J. L. Duprey, L. Giordano, J. S. Vyle, Z. Y. Zhao and J. H. Tucker, *J. Am. Chem. Soc.*, 2012, **134**, 10791–10794.

14 P. Kissel, D. J. Murray, W. J. Wulftange, V. J. Catalano and B. T. King, *Nat. Chem.*, 2014, **6**, 774–778.

15 S. Telitel, E. Blasco, L. D. Bangert, F. H. Schacher, A. S. Goldmann and C. Barner-Kowollik, *Polym. Chem.*, 2017, **8**, 4038–4042.

16 (*a*) T. K. Claus, S. Telitel, A. Welle, M. Bastmeyer, A. P. Vogt, G. Delaittre and C. Barner-Kowollik, *Chem. Commun.*, 2017, **53**, 1599–1602; (*b*) L. A. Connal, R. Vestberg, C. J. Hawker and G. G. Qiao, *Adv. Funct. Mater.*, 2008, **18**, 3315–3322.

17 P. Froimowicz, H. Frey and K. Landfester, *Macromol. Rapid Commun.*, 2011, **32**, 468–473.

18 (*a*) H. Frisch, F. R. Bloesser and C. Barner-Kowollik, *Angew. Chem., Int. Ed.*, 2019, **58**, 3604–3609; (*b*) P. Frank, A. Prasher, B. Tuten, D. Chao and E. Berda, *Appl. Petrochem. Res.*, 2015, **5**, 9–17.

19 (*a*) Z.-A. Huang, C. Chen, X.-D. Yang, X.-B. Fan, W. Zhou, C.-H. Tung, L.-Z. Wu and H. Cong, *J. Am. Chem. Soc.*, 2016, **138**, 11144–11147; (*b*) W. Xu, X.-D. Yang, X.-B. Fan, X. Wang, C.-H. Tung, L.-Z. Wu and H. Cong, *Angew. Chem., Int. Ed.*, 2019, **58**, 3943–3947.

20 (*a*) B. Gole, B. Kauffmann, V. Maurizot, I. Huc and Y. Ferrand, *Angew. Chem., Int. Ed.*, 2019, **58**, 8063–8067; (*b*) A. Wakai, H. Fukasawa, C. Yang, T. Mori and Y. Inoue, *J. Am. Chem. Soc.*, 2012, **134**, 4990–4997; (*c*) A. Urushima, D. Taura, M. Tanaka, N. Horimoto, J. Tanabe, N. Ousaka, T. Mori and E. Yashima, *Angew. Chem., Int. Ed.*, 2020, **59**, 7478–7486.

21 (*a*) L.-Y. Sun, N. Sinha, T. Yan, Y.-S. Wang, T. T. Y. Tan, L. Yu, Y.-F. Han and F. E. Hahn, *Angew. Chem., Int. Ed.*, 2018, **57**, 5161–5165; (*b*) L.-L. Ma, Y.-Y. An, L.-Y. Sun, Y.-Y. Wang, F. E. Hahn and Y.-F. Han, *Angew. Chem., Int. Ed.*, 2019, **58**, 3986–3991; (*c*) L. Zhang, R. Das, C.-T. Li, Y.-Y. Wang, F. E. Hahn, K. Hua, L.-Y. Sun and Y.-F. Han, *Angew. Chem., Int. Ed.*, 2019, **58**, 13360–13364; (*d*) Y. Li, Y.-Y. An, J.-Z. Fan,

X.-X. Liu, X. Li, F. E. Hahn, Y.-Y. Wang and Y.-F. Han, *Angew. Chem., Int. Ed.*, 2020, **59**, 10073–10080.

22 G. M. J. Schmidt, *Pure Appl. Chem.*, 1971, **27**, 647–678.

23 See for example: (*a*) E. Berni, C. Dolain, B. Kauffmann, J.-M. Léger, C.-L. Zhan and I. Huc, *J. Org. Chem.*, 2008, **73**, 2687–2694; (*b*) D. Jouvenot, E. C. Glazer and Y. Tor, *Org. Lett.*, 2006, **8**, 1987–1990; (*c*) X.-D. Huang, Y. Xu, K. Fan, S.-S. Bao, M. Kurmoo and L.-M. Zheng, *Angew. Chem., Int. Ed.*, 2018, **57**, 8577–8581.